

First Measurement of the $\Lambda_c^+ \rightarrow p\eta'$ decay

The Belle Collaboration

S. X. Li,¹⁴ J. X. Cui,¹⁴ C. P. Shen,¹⁴ I. Adachi,^{20,16} H. Aihara,⁸⁴ S. Al Said,^{79,39}
D. M. Asner,³ H. Atmacan,⁸ T. Aushev,²² R. Ayad,⁷⁹ V. Babu,⁹ P. Behera,²⁷
K. Belous,²⁹ M. Bessner,¹⁹ V. Bhardwaj,²⁴ B. Bhuyan,²⁵ T. Bilka,⁵ D. Bodrov,^{22,45}
G. Bonvicini,⁸⁸ J. Borah,²⁵ A. Bozek,⁶⁰ M. Bračko,^{49,36} P. Branchini,³²
T. E. Browder,¹⁹ A. Budano,³² M. Campajola,^{31,56} D. Červenkov,⁵ M.-C. Chang,¹³
P. Chang,⁵⁹ V. Chekelian,⁵⁰ A. Chen,⁵⁸ B. G. Cheon,¹⁸ K. Chilikin,⁴⁵ H. E. Cho,¹⁸
K. Cho,⁴¹ S.-J. Cho,⁹⁰ S.-K. Choi,⁷ Y. Choi,⁷⁷ S. Choudhury,³⁴ D. Cinabro,⁸⁸
S. Cunliffe,⁹ S. Das,⁴⁸ N. Dash,²⁷ G. De Nardo,^{31,56} G. De Pietro,³² R. Dhamija,²⁶
F. Di Capua,^{31,56} Z. Doležal,⁵ T. V. Dong,¹¹ D. Epifanov,^{4,64} T. Ferber,⁹
D. Ferlewicz,⁵¹ B. G. Fulsom,⁶⁶ R. Garg,⁶⁷ V. Gaur,⁸⁷ N. Gabyshev,^{4,64} A. Giri,²⁶
P. Goldenzweig,³⁷ B. Golob,^{46,36} E. Graziani,³² T. Gu,⁶⁸ T. Hara,^{20,16} K. Hayasaka,⁶²
H. Hayashii,⁵⁷ W.-S. Hou,⁵⁹ K. Inami,⁵⁵ A. Ishikawa,^{20,16} M. Iwasaki,⁶⁵ Y. Iwasaki,²⁰
W. W. Jacobs,²⁸ E.-J. Jang,¹⁷ S. Jia,¹⁴ Y. Jin,⁸⁴ K. K. Joo,⁶ J. Kahn,³⁷
A. B. Kaliyar,⁸⁰ K. H. Kang,³⁸ Y. Kato,⁵⁵ T. Kawasaki,⁴⁰ H. Kichimi,²⁰ C. Kiesling,⁵⁰
C. H. Kim,¹⁸ D. Y. Kim,⁷⁶ Y.-K. Kim,⁹⁰ K. Kinoshita,⁸ P. Kodyš,⁵ T. Konno,⁴⁰
A. Korobov,^{4,64} S. Korpar,^{49,36} E. Kovalenko,^{4,64} P. Krizan,^{46,36} R. Kroeger,⁵²
P. Krokovny,^{4,64} M. Kumar,⁴⁸ R. Kumar,⁶⁹ K. Kumara,⁸⁸ Y.-J. Kwon,⁹⁰ T. Lam,⁸⁷
M. Laurenza,^{32,72} S. C. Lee,⁴³ J. Li,⁴³ L. K. Li,⁸ Y. Li,¹⁴ L. Li Gioi,⁵⁰ J. Libby,²⁷
D. Liventsev,^{88,20} A. Martini,⁹ M. Masuda,^{83,70} T. Matsuda,⁵³ D. Matvienko,^{4,64,45}
S. K. Maurya,²⁵ F. Meier,¹⁰ M. Merola,^{31,56} K. Miyabayashi,⁵⁷ R. Mizuk,^{45,22}
R. Mussa,³³ M. Nakao,^{20,16} D. Narwal,²⁵ Z. Natkaniec,⁶⁰ A. Natochii,¹⁹ L. Nayak,²⁶
N. K. Nisar,³ S. Nishida,^{20,16} K. Nishimura,¹⁹ K. Ogawa,⁶² S. Ogawa,⁸¹ H. Ono,^{61,62}
P. Oskin,⁴⁵ P. Pakhlov,^{45,54} G. Pakhlova,^{22,45} T. Pang,⁶⁸ S. Pardi,³¹ S.-H. Park,²⁰
S. Patra,²⁴ T. K. Pedlar,⁴⁷ R. Pestotnik,³⁶ L. E. Piilonen,⁸⁷ T. Podobnik,^{46,36}
V. Popov,²² M. T. Prim,² M. Röhrken,⁹ A. Rostomyan,⁹ N. Rout,²⁷ G. Russo,⁵⁶
D. Sahoo,³⁴ S. Sandilya,²⁶ A. Sangal,⁸ T. Sanuki,⁸² V. Savinov,⁶⁸ G. Schnell,^{1,23}
J. Schueler,¹⁹ C. Schwanda,³⁰ A. J. Schwartz,⁸ Y. Seino,⁶² K. Senyo,⁸⁹
M. E. Sevier,⁵¹ M. Shapkin,²⁹ C. Sharma,⁴⁸ V. Shebalin,¹⁹ J.-G. Shiu,⁵⁹
B. Shwartz,^{4,64} F. Simon,⁵⁰ E. Solovieva,⁴⁵ S. Stanič,⁶³ M. Starič,³⁶ Z. S. Stottler,⁸⁷
M. Sumihama,^{15,70} K. Sumisawa,^{20,16} T. Sumiyoshi,⁸⁶ W. Sutcliffe,²
M. Takizawa,^{74,21,71} U. Tamponi,³³ K. Tanida,³⁵ F. Tenchini,⁹ K. Trabelsi,⁴⁴
M. Uchida,⁸⁵ Y. Unno,¹⁸ K. Uno,⁶² S. Uno,^{20,16} P. Urquijo,⁵¹ S. E. Vahsen,¹⁹
R. Van Tonder,² G. Varner,¹⁹ A. Vinokurova,^{4,64} E. Waheed,²⁰ D. Wang,¹²
E. Wang,⁶⁸ M.-Z. Wang,⁵⁹ S. Watanuki,⁹⁰ E. Won,⁴² X. Xu,⁷⁵ B. D. Yabsley,⁷⁸
W. Yan,⁷³ H. Ye,⁹ J. H. Yin,⁴² Y. Yusa,⁶² Y. Zhai,³⁴ V. Zhilich,^{4,64} V. Zhukova,⁴⁵

- ¹*Department of Physics, University of the Basque Country UPV/EHU, 48080 Bilbao, Spain*
- ²*University of Bonn, 53115 Bonn, Germany*
- ³*Brookhaven National Laboratory, Upton, New York 11973, USA*
- ⁴*Budker Institute of Nuclear Physics SB RAS, Novosibirsk 630090, Russian Federation*
- ⁵*Faculty of Mathematics and Physics, Charles University, 121 16 Prague, The Czech Republic*
- ⁶*Chonnam National University, Gwangju 61186, South Korea*
- ⁷*Chung-Ang University, Seoul 06974, South Korea*
- ⁸*University of Cincinnati, Cincinnati, OH 45221, USA*
- ⁹*Deutsches Elektronen-Synchrotron, 22607 Hamburg, Germany*
- ¹⁰*Duke University, Durham, NC 27708, USA*
- ¹¹*Institute of Theoretical and Applied Research (ITAR), Duy Tan University, Hanoi 100000, Vietnam*
- ¹²*University of Florida, Gainesville, FL 32611, USA*
- ¹³*Department of Physics, Fu Jen Catholic University, Taipei 24205, Taiwan*
- ¹⁴*Key Laboratory of Nuclear Physics and Ion-beam Application (MOE) and Institute of Modern Physics, Fudan University, Shanghai 200443, PR China*
- ¹⁵*Gifu University, Gifu 501-1193, Japan*
- ¹⁶*SOKENDAI (The Graduate University for Advanced Studies), Hayama 240-0193, Japan*
- ¹⁷*Gyeongsang National University, Jinju 52828, South Korea*
- ¹⁸*Department of Physics and Institute of Natural Sciences, Hanyang University, Seoul 04763, South Korea*
- ¹⁹*University of Hawaii, Honolulu, HI 96822, USA*
- ²⁰*High Energy Accelerator Research Organization (KEK), Tsukuba 305-0801, Japan*
- ²¹*J-PARC Branch, KEK Theory Center, High Energy Accelerator Research Organization (KEK), Tsukuba 305-0801, Japan*
- ²²*National Research University Higher School of Economics, Moscow 101000, Russian Federation*
- ²³*IKERBASQUE, Basque Foundation for Science, 48013 Bilbao, Spain*
- ²⁴*Indian Institute of Science Education and Research Mohali, SAS Nagar, 140306, India*
- ²⁵*Indian Institute of Technology Guwahati, Assam 781039, India*
- ²⁶*Indian Institute of Technology Hyderabad, Telangana 502285, India*
- ²⁷*Indian Institute of Technology Madras, Chennai 600036, India*
- ²⁸*Indiana University, Bloomington, IN 47408, USA*
- ²⁹*Institute for High Energy Physics, Protvino 142281, Russian Federation*
- ³⁰*Institute of High Energy Physics, Vienna 1050, Austria*
- ³¹*INFN - Sezione di Napoli, I-80126 Napoli, Italy*
- ³²*INFN - Sezione di Roma Tre, I-00146 Roma, Italy*
- ³³*INFN - Sezione di Torino, I-10125 Torino, Italy*
- ³⁴*Iowa State University, Ames, Iowa 50011, USA*
- ³⁵*Advanced Science Research Center, Japan Atomic Energy Agency, Naka 319-1195, Japan*
- ³⁶*J. Stefan Institute, 1000 Ljubljana, Slovenia*
- ³⁷*Institut für Experimentelle Teilchenphysik, Karlsruher Institut für Technologie, 76131 Karlsruhe, Germany*
- ³⁸*Kavli Institute for the Physics and Mathematics of the Universe (WPI), University of Tokyo, Kashiwa 277-8583, Japan*

- ³⁹*Department of Physics, Faculty of Science, King Abdulaziz University, Jeddah 21589, Saudi Arabia*
- ⁴⁰*Kitasato University, Sagamihara 252-0373, Japan*
- ⁴¹*Korea Institute of Science and Technology Information, Daejeon 34141, South Korea*
- ⁴²*Korea University, Seoul 02841, South Korea*
- ⁴³*Kyungpook National University, Daegu 41566, South Korea*
- ⁴⁴*Université Paris-Saclay, CNRS/IN2P3, IJCLab, 91405 Orsay, France*
- ⁴⁵*P.N. Lebedev Physical Institute of the Russian Academy of Sciences, Moscow 119991, Russian Federation*
- ⁴⁶*Faculty of Mathematics and Physics, University of Ljubljana, 1000 Ljubljana, Slovenia*
- ⁴⁷*Luther College, Decorah, IA 52101, USA*
- ⁴⁸*Malaviya National Institute of Technology Jaipur, Jaipur 302017, India*
- ⁴⁹*Faculty of Chemistry and Chemical Engineering, University of Maribor, 2000 Maribor, Slovenia*
- ⁵⁰*Max-Planck-Institut für Physik, 80805 München, Germany*
- ⁵¹*School of Physics, University of Melbourne, Victoria 3010, Australia*
- ⁵²*University of Mississippi, University, MS 38677, USA*
- ⁵³*University of Miyazaki, Miyazaki 889-2192, Japan*
- ⁵⁴*Moscow Physical Engineering Institute, Moscow 115409, Russian Federation*
- ⁵⁵*Graduate School of Science, Nagoya University, Nagoya 464-8602, Japan*
- ⁵⁶*Università di Napoli Federico II, I-80126 Napoli, Italy*
- ⁵⁷*Nara Women's University, Nara 630-8506, Japan*
- ⁵⁸*National Central University, Chung-li 32054, Taiwan*
- ⁵⁹*Department of Physics, National Taiwan University, Taipei 10617, Taiwan*
- ⁶⁰*H. Niewodniczanski Institute of Nuclear Physics, Krakow 31-342, Poland*
- ⁶¹*Nippon Dental University, Niigata 951-8580, Japan*
- ⁶²*Niigata University, Niigata 950-2181, Japan*
- ⁶³*University of Nova Gorica, 5000 Nova Gorica, Slovenia*
- ⁶⁴*Novosibirsk State University, Novosibirsk 630090, Russian Federation*
- ⁶⁵*Osaka City University, Osaka 558-8585, Japan*
- ⁶⁶*Pacific Northwest National Laboratory, Richland, WA 99352, USA*
- ⁶⁷*Panjab University, Chandigarh 160014, India*
- ⁶⁸*University of Pittsburgh, Pittsburgh, PA 15260, USA*
- ⁶⁹*Punjab Agricultural University, Ludhiana 141004, India*
- ⁷⁰*Research Center for Nuclear Physics, Osaka University, Osaka 567-0047, Japan*
- ⁷¹*Meson Science Laboratory, Cluster for Pioneering Research, RIKEN, Saitama 351-0198, Japan*
- ⁷²*Dipartimento di Matematica e Fisica, Università di Roma Tre, I-00146 Roma, Italy*
- ⁷³*Department of Modern Physics and State Key Laboratory of Particle Detection and Electronics, University of Science and Technology of China, Hefei 230026, PR China*
- ⁷⁴*Showa Pharmaceutical University, Tokyo 194-8543, Japan*
- ⁷⁵*Soochow University, Suzhou 215006, China*
- ⁷⁶*Soongsil University, Seoul 06978, South Korea*
- ⁷⁷*Sungkyunkwan University, Suwon 16419, South Korea*
- ⁷⁸*School of Physics, University of Sydney, New South Wales 2006, Australia*
- ⁷⁹*Department of Physics, Faculty of Science, University of Tabuk, Tabuk 71451, Saudi Arabia*

⁸⁰ *Tata Institute of Fundamental Research, Mumbai 400005, India*

⁸¹ *Toho University, Funabashi 274-8510, Japan*

⁸² *Department of Physics, Tohoku University, Sendai 980-8578, Japan*

⁸³ *Earthquake Research Institute, University of Tokyo, Tokyo 113-0032, Japan*

⁸⁴ *Department of Physics, University of Tokyo, Tokyo 113-0033, Japan*

⁸⁵ *Tokyo Institute of Technology, Tokyo 152-8550, Japan*

⁸⁶ *Tokyo Metropolitan University, Tokyo 192-0397, Japan*

⁸⁷ *Virginia Polytechnic Institute and State University, Blacksburg, VA 24061, USA*

⁸⁸ *Wayne State University, Detroit, MI 48202, USA*

⁸⁹ *Yamagata University, Yamagata 990-8560, Japan*

⁹⁰ *Yonsei University, Seoul 03722, South Korea*

ABSTRACT: We present the first measurement of the branching fraction of the singly Cabibbo-suppressed (SCS) decay $\Lambda_c^+ \rightarrow p\eta'$ with $\eta' \rightarrow \eta\pi^+\pi^-$, using a data sample corresponding to an integrated luminosity of 981 fb^{-1} , collected by the Belle detector at the KEKB e^+e^- asymmetric-energy collider. A significant $\Lambda_c^+ \rightarrow p\eta'$ signal is observed for the first time with a signal significance of 5.4σ . The relative branching fraction with respect to the normalization mode $\Lambda_c^+ \rightarrow pK^-\pi^+$ is measured to be

$$\frac{\mathcal{B}(\Lambda_c^+ \rightarrow p\eta')}{\mathcal{B}(\Lambda_c^+ \rightarrow pK^-\pi^+)} = (7.54 \pm 1.32 \pm 0.73) \times 10^{-3},$$

where the uncertainties are statistical and systematic, respectively. Using the world-average value of $\mathcal{B}(\Lambda_c^+ \rightarrow pK^-\pi^+) = (6.28 \pm 0.32) \times 10^{-2}$, we obtain

$$\mathcal{B}(\Lambda_c^+ \rightarrow p\eta') = (4.73 \pm 0.82 \pm 0.46 \pm 0.24) \times 10^{-4},$$

where the uncertainties are statistical, systematic, and from $\mathcal{B}(\Lambda_c^+ \rightarrow pK^-\pi^+)$, respectively.

Contents

1	Introduction	1
2	The Belle detector and data sample	2
3	Selection criteria	2
4	Signal and background estimation	4
5	Systematic Uncertainties	7
6	Conclusions	8

1 Introduction

Hadronic decays of charmed baryons provide an ideal laboratory to understand the interplay of weak and strong interactions in the charm system [1–3]. Decays of charmed baryons receive sizable nonfactorizable contributions from W-exchange diagrams, which are subject to color and helicity suppression [4–7]. Therefore, the study of nonfactorizable contributions is critical to understand the dynamics of charmed baryon decays. To avoid theoretical difficulties in the factorization approach [4], one can use the $SU(3)_F$ flavor symmetry to relate the amplitudes among different decays [5, 8, 9]. Other theoretical approaches provide calculations based on dynamical models [10–12]. For the singly Cabibbo-suppressed (SCS) decay $\Lambda_c^+ \rightarrow p\eta'$, theoretical predictions on its branching fraction under different assumptions vary by more than an order of magnitude as listed in table 1. Currently, this decay has not yet been observed.

Table 1. Comparison of different theoretical predictions for $\mathcal{B}(\Lambda_c^+ \rightarrow p\eta')$ (in units of 10^{-3}).

	$SU(3)_F$ symmetry [5]	$SU(3)_F$ symmetry [13]	Constituent quark model [3]
$\mathcal{B}(\Lambda_c^+ \rightarrow p\eta')$	0.4 – 0.6	$1.22^{+1.43}_{-0.87}$	0.04 – 0.2

In this study, based on an e^+e^- annihilation data sample of 981 fb^{-1} collected by the Belle experiment, we measure the branching fraction of the signal mode $\Lambda_c^+ \rightarrow p\eta'$ with respect to the normalization mode $\Lambda_c^+ \rightarrow pK^-\pi^+$. Throughout this paper, charge-conjugate modes are implicitly included unless stated otherwise. The paper is organized as follows. Section 2 introduces the Belle detector and data sample. Section 3 discusses the event selection criteria. The signal and background estimations are presented in section 4. Sections 5 and 6 describe the systematic uncertainty and conclusion, respectively.

2 The Belle detector and data sample

This measurement is based on a data sample corresponding to an integrated luminosity of 981 fb^{-1} , collected with the Belle detector at the KEKB asymmetric-energy e^+e^- collider [14, 15]. About 70% of the data were recorded at the $\Upsilon(4S)$ resonance, and the rest were collected at other $\Upsilon(nS)$ ($n = 1, 2, 3,$ or 5) states or at center-of-mass (CM) energies a few tens of MeV below the $\Upsilon(4S)$ or the $\Upsilon(nS)$ peaks.

The Belle detector is a large-solid-angle magnetic spectrometer that consists of a silicon vertex detector (SVD), a 50-layer central drift chamber (CDC), an array of aerogel threshold Cherenkov counters (ACC), a barrel-like arrangement of time-of-flight scintillation counters (TOF), and an electromagnetic calorimeter comprised of CsI(Tl) crystals (ECL) located inside a superconducting solenoid coil that provides a 1.5 T magnetic field. An iron flux-return located outside of the coil is instrumented to detect K_L^0 mesons and to identify muons. The detector is described in detail elsewhere [16, 17]. The origin of the coordinate system is defined as the position of the nominal interaction point, and the axis aligning with the direction opposite the e^+ beam is defined as the z axis.

Monte Carlo (MC) simulated events are used to optimize the selection criteria, study backgrounds, and determine the signal reconstruction efficiency. Samples of simulated signal MC events are generated by EVTGEN [18] and propagated through a detector simulation based on GEANT3 [19]. The $e^+e^- \rightarrow c\bar{c}$ events are simulated using PYTHIA [20]; the decays $\Lambda_c^+ \rightarrow pK^-\pi^+$ and $\eta' \rightarrow \eta\pi^+\pi^-$ are generated with a phase space model. We take into account the effect of final-state radiation from charged particles by using the PHOTOS package [22]. Simulated samples of $\Upsilon(4S) \rightarrow B^+B^-/B^0\bar{B}^0$, $\Upsilon(5S) \rightarrow B_s^{(*)}\bar{B}_s^{(*)}/B^{(*)}\bar{B}^{(*)}(\pi)/\Upsilon(4S)\gamma$, $e^+e^- \rightarrow q\bar{q}$ ($q = u, d, s, c$) at $\sqrt{s} = 10.52, 10.58,$ and 10.867 GeV , and $\Upsilon(1S, 2S, 3S)$ decays, normalized to the same integrated luminosity as real data, are used to develop the selection criteria and perform the background study [23].

3 Selection criteria

Selection criteria are optimized by maximizing a figure-of-merit $\epsilon/(\frac{a}{2} + \sqrt{n_B})$ [24], where ϵ is the signal efficiency; a is the target signal significance expressed in standard deviations in a one-sided Gaussian test, selected to be 5; n_B is the number of background events expected in a two-dimensional signal region of η' and Λ_c^+ signals, which is defined as $(0.95, 0.965) \text{ GeV}/c^2$ in $M(\eta\pi^+\pi^-)$ and $(2.27, 2.31) \text{ GeV}/c^2$ in $M(p\eta')$.

We reconstruct the decays $\Lambda_c^+ \rightarrow p\eta'$ and $\Lambda_c^+ \rightarrow pK^-\pi^+$, with the η' decay reconstructed in the cascade $\eta\pi^+\pi^-$, $\eta \rightarrow \gamma\gamma$. Final-state charged tracks are identified as $p, K,$ or π candidates using information from the charged-hadron identification systems (ACC, TOF, CDC) combined into a likelihood ratio, $\mathcal{R}(h|h') = \mathcal{L}(h)/(\mathcal{L}(h) + \mathcal{L}(h'))$ where h and h' are $\pi, K,$ or p as appropriate [25]. Tracks having $\mathcal{R}(p|\pi) > 0.9$ and $\mathcal{R}(p|K) > 0.9$ are identified as proton candidates; charged kaon candidates are required to have $\mathcal{R}(K|p) > 0.4$ and $\mathcal{R}(K|\pi) > 0.9$; and charged pion candidates to have $\mathcal{R}(\pi|p) > 0.4$ and $\mathcal{R}(\pi|K) > 0.4$. A likelihood ratio for electron identification, $\mathcal{R}(e)$, is formed from ACC, CDC, and ECL information [26], and is required to be less than 0.9 for all charged tracks to suppress elec-

trons. The identification efficiencies of p , K , and π are 82%, 70%, and 97%, respectively. The probabilities of misidentifying h as h' , $P(h \rightarrow h')$, are estimated to be 3% [$P(p \rightarrow \pi)$], 7% [$P(p \rightarrow K)$], 10% [$P(K \rightarrow \pi)$], 2% [$P(K \rightarrow p)$], 5% [$P(\pi \rightarrow K)$], and 1% [$P(\pi \rightarrow p)$]. For each charged track, the distance of the closest approach with respect to the interaction point along the z axis and in the transverse $x - y$ plane is required to be less than 2.0 cm and 0.1 cm, respectively. Each track must have at least one SVD hit in both the z direction and the $x - y$ plane.

Photon candidates are selected from ECL clusters not associated with any charged tracks. The photon energy is required to be greater than 90 MeV in the barrel region ($-0.63 < \cos\theta < 0.85$) and greater than 120 MeV in the endcap region ($-0.91 < \cos\theta < -0.63$ or $0.85 < \cos\theta < 0.98$) of the ECL, where θ is the polar angle relative to the positive z axis. To reject neutral hadrons, the ratio of the energy deposited in the central 3×3 array of ECL crystals to the total energy deposited in the enclosing 5×5 array of crystals is required to be at least 0.9 for each photon candidate.

The η candidates are reconstructed via their decay to two photons. The $\gamma\gamma$ invariant mass is required to satisfy $0.45 < M(\gamma\gamma) < 0.65 \text{ GeV}/c^2$, and then a mass-constrained fit is performed for η candidates to improve the momentum resolution. The corresponding χ^2 value of the mass-constrained fit on η (χ_η^2) is required to be less than 10. To further suppress background events, we remove η candidates in which either of the daughter photons can be combined with other photons in the event to form $\pi^0 \rightarrow \gamma\gamma$ candidates satisfying $|M(\gamma\gamma) - m_{\pi^0}| \ll 12 \text{ MeV}/c^2$, where m_{π^0} is the nominal π^0 mass [21]. With this veto, we reject 42% of the background, while retaining 83% of the signal.

The η' candidates are reconstructed by combining two opposite-charge π tracks with an η candidate. The invariant mass distribution of $\eta\pi^+\pi^-$ from data is shown in figure 1. Candidates η' are retained if $0.950 < M(\eta\pi^+\pi^-) < 0.965 \text{ GeV}/c^2$, corresponding to an efficiency of 96%. The η' sidebands are defined as 0.915 to 0.930 GeV/c^2 and 0.980 to 0.995 GeV/c^2 , which are the regions between two blue lines in the $M(\eta\pi^+\pi^-)$ distribution.

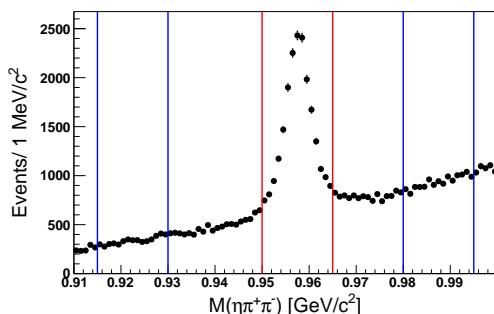


Figure 1. The invariant mass distribution of $\eta\pi^+\pi^-$. The region between two red lines is selected as the η' signal region, and the regions between two blue lines are the η' sidebands.

Candidates for $\Lambda_c^+ \rightarrow pK^-\pi^+$ and $\Lambda_c^+ \rightarrow p\eta'$ decays are reconstructed by combining p , K^- , π^+ candidates, and p , η' candidates, respectively. A vertex fit is performed with

the three charged tracks to suppress combinatorial background events. The resulting fit quality is labeled χ_{vtx}^2 . For $\Lambda_c^+ \rightarrow pK^-\pi^+$, the χ_{vtx}^2 is required to be less than 40, while for $\Lambda_c^+ \rightarrow p\eta'$, $\chi_{\text{vtx}}^2 < 15$ is required. For both χ_{vtx}^2 requirements, the efficiency is larger than 98%. A scaled momentum of $x_p > 0.53$ is required to suppress background, especially from B -meson decays, where $x_p = p^*/\sqrt{E_{\text{cm}}^2/4c^2 - M^2c^2}$, E_{cm} is the CM energy, and p^* and M are the momentum and invariant mass, respectively, of the Λ_c^+ candidates in the CM frame.

After the preliminary selection, about 0.8% of the $\Lambda_c^+ \rightarrow pK^-\pi^+$ events and 13.3% of the $\Lambda_c^+ \rightarrow p\eta'$ events have two or more Λ_c^+ candidates. We choose the best η candidate according to the smallest value of χ_{η}^2 ; the rate of events having multiple $\Lambda_c^+ \rightarrow p\eta'$ candidates with this criterion is 1.6%. For such multi-candidate events, we choose a single Λ_c^+ candidate randomly. This best-candidate selection, based on the MC simulation, identifies the correct candidate 65% of the time. The $p\eta'$ mass distribution for wrong-combination simulated signal events is found to be smooth. We keep all candidates of $\Lambda_c^+ \rightarrow pK^-\pi^+$ in multiple-candidate events as the multiplicity is negligible.

4 Signal and background estimation

With the above selection criteria applied, the invariant mass distributions of normalization and signal modes are shown in figure 2. From a study of generic MC samples [23], no known peaking background processes contribute to mass distributions in the Λ_c^+ signal region.

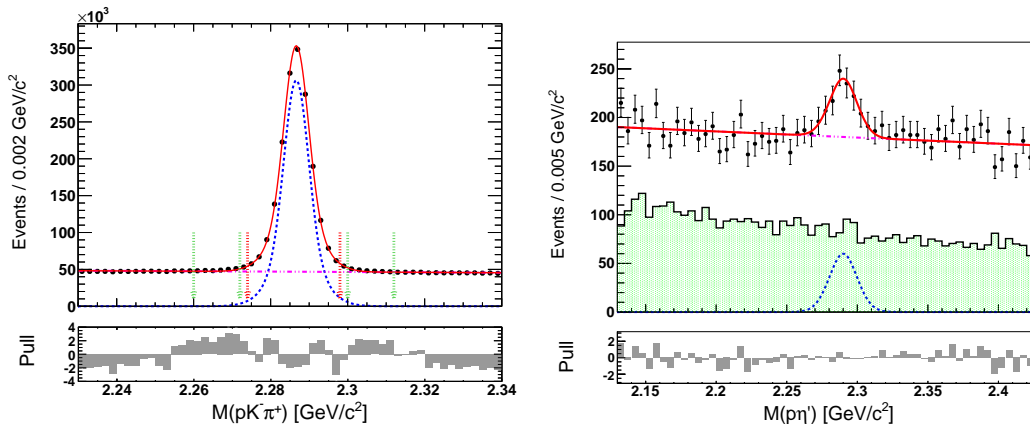


Figure 2. Fits to the invariant mass distributions of the $pK^-\pi^+$ (Left) and $p\eta'$ combinations (Right). Black dots with error bars represent the data; red solid lines represent the total fitted result; blue dashed lines represent the signal shape; magenta dot-dashed lines represent the background shape; and the green histogram is from normalized η' sidebands.

To extract the number of signal events, we perform an unbinned maximum-likelihood fit to the $M(pK^-\pi^+)$ or $M(p\eta')$ distribution. The likelihood function is defined in terms

of a signal PDF (F_S) and a background PDF (F_B) as

$$\mathcal{L} = \frac{e^{-(n_S+n_B)}}{N!} \prod_i^N [n_S F_S(M_i) + n_B F_B(M_i)], \quad (4.1)$$

where N is the total number of observed events; n_S and n_B are the numbers of signal events and background events, respectively; M is $pK^-\pi^+$ or $p\eta'$ invariant mass; and i denotes the event index. The fit is performed to candidate events surviving the selection criteria; n_S and n_B are free parameters in the fit.

For the $\Lambda_c^+ \rightarrow pK^-\pi^+$ channel, we extract the Λ_c^+ signal yields by fitting the $M(pK^-\pi^+)$ distribution. The signal PDF is a sum of two Gaussian functions with a common mean, and the background PDF is a second-order polynomial. All parameters of F_S and F_B are floated. The fit result is shown in figure 2 (Left), along with the pull distribution. The fitted signal yield is $N_{\text{norm}} = 1472190 \pm 5726$, where the uncertainty is statistical. From the MC simulation, the mass resolution for $\Lambda_c^+ \rightarrow pK^-\pi^+$ is $8 \text{ MeV}/c^2$.

For the $\Lambda_c^+ \rightarrow p\eta'$ channel, we first check the $M(p\pi^+\pi^-\eta)$ distribution from normalized η' sidebands, as shown in figure 2 (Right). The distribution from the normalized η' sidebands is smoothly falling, indicating a negligible contribution from $\Lambda_c^+ \rightarrow p\pi^+\pi^-\eta$ decays. We subsequently fit the $M(p\eta')$ distribution to extract the Λ_c^+ signal yield. A sum of a Gaussian function and a Crystal Ball (CB) function [27] is used as the signal PDF, and a second-order polynomial as the background PDF. The Gaussian and CB functions are fixed to have a common mean. All other parameters are floated in the fit. The fit result, along with the pull distribution, is shown in figure 2 (Right). A clear Λ_c^+ signal is observed in the $M(p\eta')$ distribution. The fitted signal yield is $N_{\text{sig}} = 294 \pm 52$, where the uncertainty is statistical. The mass resolution for $\Lambda_c^+ \rightarrow p\eta'$ is $13 \text{ MeV}/c^2$ from the MC simulation, which is the half-width at half maximum. The statistical significance of the Λ_c^+ signal is 6.3σ , calculated from the difference of the logarithmic likelihoods, $-2\ln(\mathcal{L}_0/\mathcal{L}_{\text{max}}) = 59.2$, where \mathcal{L}_0 and \mathcal{L}_{max} are the maximized likelihoods without and with a signal component, respectively [28]. The significance takes into account the difference in the number of degrees of freedom in the two fits ($\Delta ndf=7$). Since the largest systematic uncertainty is due to the fit, as described in section 5, alternative fits to the $M(p\eta')$ spectrum under different fit conditions are performed and the Λ_c^+ signal significance is larger than 5.4σ in all cases.

To measure the branching fraction, we must divide these extracted signal yields by their reconstruction efficiencies. Since $\Lambda_c^+ \rightarrow p\eta'$ is a two-body decay and $\eta' \rightarrow \eta\pi^+\pi^-$ is well modeled by the phase space [29], we estimate the reconstruction efficiency directly from the simulated events by the ratio $n_{\text{sel}}/n_{\text{gen}}$, where n_{sel} and n_{gen} are the numbers of true signal events surviving the selection criteria and generated events, respectively. The signal mode reconstruction efficiency is determined to be $\epsilon_{\text{sig}} = (2.22 \pm 0.02)\%$. However, the reconstruction efficiency for the decay $\Lambda_c^+ \rightarrow pK^-\pi^+$ can vary across the three-body phase space, as visualized in a Dalitz plot [30] with polarization neglected. To take this into account, we correct the reconstruction efficiency according to the Dalitz plot from data as follows. Figure 3 shows the Dalitz distribution of $M^2(pK^-)$ versus $M^2(K^-\pi^+)$ in the $\Lambda_c^+ \rightarrow pK^-\pi^+$ signal region from data which is defined as $2.274 < M(pK^-\pi^+) < 2.298$

GeV/ c^2 . The number of background events has been subtracted using the normalized Λ_c^+ sidebands defined as (2.260, 2.272) GeV/ c^2 and (2.300, 2.312) GeV/ c^2 . The effect of the variation of the kinematic boundaries with $M(pK^-\pi^+)$ is neglected. We divide the Dalitz plot for the data into 120×120 bins, with a bin size of 0.027 GeV $^2/c^4$ for $M^2(pK^-)$ and 0.016 GeV $^2/c^4$ for $M^2(K^-\pi^+)$. The corrected reconstruction efficiency is determined via

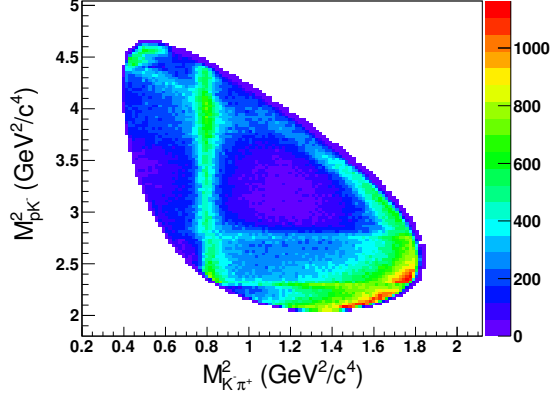


Figure 3. Dalitz plot of the selected $\Lambda_c^+ \rightarrow pK^-\pi^+$ candidates.

the formula

$$\epsilon_{\text{norm}}^{\text{corr}} = \frac{\sum_i s_i}{\sum_j (s_j / \epsilon_j)}, \quad (4.2)$$

where i and j run over all bins; $\sum_i s_i$ is the number of signal candidates in data; s_j and ϵ_j are the number of signal candidates in data and the reconstruction efficiency from MC simulation events for each bin, respectively. The reconstruction efficiency for each bin is obtained by dividing the number of signal events after applying the selection criteria by the number of generated events. The corrected reconstruction efficiency is $\epsilon_{\text{norm}}^{\text{corr}} = (14.06 \pm 0.01)\%$.

The branching fraction of the signal mode relative to that of the normalization mode is determined via

$$\frac{\mathcal{B}(\Lambda_c^+ \rightarrow p\eta')}{\mathcal{B}(\Lambda_c^+ \rightarrow pK^-\pi^+)} = \frac{N_{\text{sig}}/\epsilon_{\text{sig}}}{N_{\text{norm}}/\epsilon_{\text{norm}}^{\text{corr}}} \times \frac{1}{\mathcal{B}'}, \quad (4.3)$$

where $\mathcal{B}' = \mathcal{B}(\eta' \rightarrow \eta\pi^+\pi^-) \times \mathcal{B}(\eta \rightarrow \gamma\gamma)$ [21]. Inserting all extracted signal yields and reconstruction efficiencies into eq. (4.3) gives the branching fraction ratio

$$\frac{\mathcal{B}(\Lambda_c^+ \rightarrow p\eta')}{\mathcal{B}(\Lambda_c^+ \rightarrow pK^-\pi^+)} = (7.54 \pm 1.32 \pm 0.73) \times 10^{-3}, \quad (4.4)$$

where the first error is statistical and the second is systematic, as evaluated in section 5. Multiplying both sides of eq. (4.4) by the world average value $\mathcal{B}(\Lambda_c^+ \rightarrow pK^-\pi^+) = (6.28 \pm 0.32) \times 10^{-2}$ [21] gives

$$\mathcal{B}(\Lambda_c^+ \rightarrow p\eta') = (4.73 \pm 0.82 \pm 0.46 \pm 0.24) \times 10^{-4}, \quad (4.5)$$

Table 2. The sources of the relative systematic uncertainties (%) in the measurement of the ratio of branching fractions.

Source	Systematic uncertainties (%)
PID efficiency	3.5
Photon efficiency	4.0
η' mass window	0.8
Best-candidate selection	1.2
Normalization mode fit	1.8
Signal mode fit	7.6
\mathcal{B}'	1.3
Signal MC sample size	0.7
Total	9.7

where the third uncertainty is from the uncertainty in $\mathcal{B}(\Lambda_c^+ \rightarrow pK^-\pi^+)$.

5 Systematic Uncertainties

Table 2 summarizes the sources of systematic uncertainties in measuring the ratio of branching fractions. These uncertainties are assessed as follows.

- The momentum and angular distributions of protons from $\Lambda_c^+ \rightarrow pK^-\pi^+$ and $\Lambda_c^+ \rightarrow p\eta'$ are similar. Based on the study of inclusive Λ decay $\Lambda \rightarrow p\eta'$, the uncertainty from PID efficiency of the proton is below 0.1% and is therefore neglected. For the pion with the same charge in the numerator and denominator of eq. (4.4), the uncertainties in PID efficiencies only partially cancel because of differences in momentum distributions; Using a control sample of $D^{*+} \rightarrow D^0\pi^+$ with $D^0 \rightarrow K^-\pi^+$ decay, we assign an uncertainty of 0.7%. Uncertainties of 1.6% and 1.2% are assigned for the K and remaining π identification efficiencies, respectively. The total systematic uncertainty from PID is 3.5%, adding individual PID uncertainties linearly as they are highly correlated.
- Based on a study of radiative Bhabha events, a systematic uncertainty of 2.0% is assigned to the photon efficiency for each photon, and the total systematic uncertainty from photon reconstruction is thus 4.0%.
- The efficiency of the requirement on $M(\eta\pi^+\pi^-)$ is 96.3% for data and 97.1% for MC simulation, with a ratio of 99.2%. We take the relative difference on efficiencies between data and MC simulation as the uncertainty due to the η' mass window, which is 0.8%.
- The uncertainty from the best-candidate selection is estimated by turning off the multiple candidate rejection and the difference in branching fraction ratio without best-candidate selection relative to the nominal one is taken as the uncertainty, which is 1.2%.

- Uncertainties from the fits are estimated by modifying the forms of F_S and F_B , and enlarging the fit range.
 - To evaluate the uncertainty from the fit of the normalization mode, the signal PDF used is a sum of three Gaussian functions with a common mean, and the background PDF used is a first-order polynomial. The fit range is enlarged to be (2.15, 2.42) GeV/ c^2 . The difference in signal yields is taken as the uncertainty. We sum these contributions in quadrature to obtain a 1.8% uncertainty.
 - To evaluate the uncertainty from the fit of the signal mode, the signal PDF is changed to a sum of two CB functions, and the background PDF is changed to a third-order polynomial. We also enlarge the fit range. Moreover, we perform a simultaneous fit to the $M(p\pi^+\pi^-\eta)$ distributions from the selected events in the η' signal region and the normalized η' sidebands to estimate the contribution from a possible $\Lambda_c^+ \rightarrow p\pi^+\pi^-\eta$ non-resonant component. The difference in signal yields from each change is taken as the uncertainty. We sum these contributions in quadrature to obtain a 7.6% uncertainty.
- The uncertainty on the product of the branching fractions of the decays $\eta' \rightarrow \eta\pi^+\pi^-$ and $\eta \rightarrow \gamma\gamma$ is 1.3% [21].
- Uncertainty from the finite statistics of the signal MC samples is 0.7%.
- Since there are three charged tracks in the final states both for normalization mode and signal mode, the uncertainty due to the tracking efficiency largely cancels in the ratio. For the normalization mode, the reconstruction efficiency is corrected by the Dalitz plot of the data; the uncertainty from the generator model is therefore negligible. For the signal mode, since the signal efficiency does not depend on the angular distribution of the proton in the Λ_c^+ rest frame, the model-dependent uncertainty has a negligible effect on the efficiency. For the decay $\eta' \rightarrow \eta\pi^+\pi^-$, the internal dynamics is very similar to the phase space [29], thus the systematic uncertainty from the generator model of $\eta' \rightarrow \eta\pi^+\pi^-$ is ignored.

The total systematic uncertainty is obtained by adding in quadrature all the above contributions. The results are listed in table 2.

6 Conclusions

In summary, using the full Belle data set corresponding to an integrated luminosity of 981 fb $^{-1}$, we present the first measurement of the branching fraction of $\Lambda_c^+ \rightarrow p\eta'$ relative to that of $\Lambda_c^+ \rightarrow pK^-\pi^+$. The decay $\Lambda_c^+ \rightarrow p\eta'$ is observed with a significance of 5.4σ . Our result is

$$\frac{\mathcal{B}(\Lambda_c^+ \rightarrow p\eta')}{\mathcal{B}(\Lambda_c^+ \rightarrow pK^-\pi^+)} = (7.54 \pm 1.32(\text{stat}) \pm 0.73(\text{syst})) \times 10^{-3}.$$

Inserting the world average value $\mathcal{B}(\Lambda_c^+ \rightarrow pK^-\pi^+) = (6.28 \pm 0.32) \times 10^{-2}$ [21] gives the absolute branching fraction

$$\mathcal{B}(\Lambda_c^+ \rightarrow p\eta') = (4.73 \pm 0.82(\text{stat}) \pm 0.46(\text{syst}) \pm 0.24(\text{ref})) \times 10^{-4},$$

where the uncertainties are statistical, systematic, and from $\mathcal{B}(\Lambda_c^+ \rightarrow pK^-\pi^+)$, respectively. Our result is consistent with theoretical calculations based on $SU(3)_F$ symmetry [5, 13], while not consistent with a constituent quark model prediction [3].

Acknowledgments

We thank the KEKB group for the excellent operation of the accelerator; the KEK cryogenics group for the efficient operation of the solenoid; and the KEK computer group, and the Pacific Northwest National Laboratory (PNNL) Environmental Molecular Sciences Laboratory (EMSL) computing group for strong computing support; and the National Institute of Informatics, and Science Information NETwork 5 (SINET5) for valuable network support. We acknowledge support from the Ministry of Education, Culture, Sports, Science, and Technology (MEXT) of Japan, the Japan Society for the Promotion of Science (JSPS), and the Tau-Lepton Physics Research Center of Nagoya University; the Australian Research Council including grants DP180102629, DP170102389, DP170102204, DP150103061, FT130100303; Austrian Federal Ministry of Education, Science and Research (FWF) and FWF Austrian Science Fund No. P 31361-N36; the National Natural Science Foundation of China under Contracts No. 11475187, No. 11521505, No. 11575017, No. 11675166, No. 11705209, No. 12005040, No. 11761141009, No. 11975076, No. 12042509, No. 12135005, No. 12161141008; Key Research Program of Frontier Sciences, Chinese Academy of Sciences (CAS), Grant No. QYZDJ-SSW-SLH011; the CAS Center for Excellence in Particle Physics (CCEPP); the Shanghai Science and Technology Committee (STCSM) under Grant No. 19ZR1403000; the Ministry of Education, Youth and Sports of the Czech Republic under Contract No. LTT17020; Horizon 2020 ERC Advanced Grant No. 884719 and ERC Starting Grant No. 947006 “InterLeptons” (European Union); the Carl Zeiss Foundation, the Deutsche Forschungsgemeinschaft, the Excellence Cluster Universe, and the VolkswagenStiftung; the Department of Atomic Energy (Project Identification No. RTI 4002) and the Department of Science and Technology of India; the Istituto Nazionale di Fisica Nucleare of Italy; National Research Foundation (NRF) of Korea Grant Nos. 2016R1D1A1B01010135, 2016R1D1A1B02012900, 2018R1A2B3003643, 2018R1A6A1A06024970, 2019K1A3A7A09033840, 2019R1I1A3A01058933, 2021R1A6A1A-03043957, 2021R1F1A1060423, 2021R1F1A1064008; Radiation Science Research Institute, Foreign Large-size Research Facility Application Supporting project, the Global Science Experimental Data Hub Center of the Korea Institute of Science and Technology Information and KREONET/GLORIAD; the Polish Ministry of Science and Higher Education and the National Science Center; the Ministry of Science and Higher Education of the Russian Federation, Agreement 14.W03.31.0026, and the HSE University Basic Research Program, Moscow; University of Tabuk research grants S-1440-0321, S-0256-1438, and S-0280-1439

(Saudi Arabia); the Slovenian Research Agency Grant Nos. J1-9124 and P1-0135; Ikerbasque, Basque Foundation for Science, Spain; the Swiss National Science Foundation; the Ministry of Education and the Ministry of Science and Technology of Taiwan; and the United States Department of Energy and the National Science Foundation.

References

- [1] B. Andersson, G. Gustafson, G. Ingelman, and T. Sjöstrand, *Parton fragmentation and string dynamics*, *Phys. Rep.* **97** (1983) 31.
- [2] B. Andersson, G. Gustafson, and T. Sjöstrand, *Baryon production in jet fragmentation and Υ -decay*, *Phys. Scr.* **32** (1985) 574.
- [3] T. Uppal, R. C. Verma, and M. P. Khanna, *Constituent quark model analysis of weak mesonic decays of charm baryons*, *Phys. Rev. D* **49** (1994) 3417.
- [4] P. Zenczykowski, *Quark and pole models of nonleptonic decays of charmed baryons*, *Phys. Rev. D* **50** (1994) 402.
- [5] K. K. Sharma and R. C. Verma, *$SU(3)_{\text{flavor}}$ analysis of two-body weak decays of charmed baryons*, *Phys. Rev. D* **55** (1997) 7067.
- [6] M. A. Ivanov, J. G. Korner, V. E. Lyubovitskij, and A. G. Rusetsky, *Exclusive nonleptonic decays of bottom and charm baryons in a relativistic three-quark model: Evaluation of nonfactorizing diagrams*, *Phys. Rev. D* **57** (1998) 5632.
- [7] Y. Kohara, *Two-body nonleptonic decays of charmed baryons*, *Nuovo Cim. A* **111** (1998) 67.
- [8] M. J. Savage and R. P. Springer, *$SU(3)$ predictions for charmed-baryon decays*, *Phys. Rev. D* **42** (1990) 1527.
- [9] M. J. Savage, *$SU(3)$ violations in the nonleptonic decay of charmed hadrons*, *Phys. Lett. B* **257** (1991) 414.
- [10] H. Y. Cheng, X. W. Kang, and F. R. Xu, *Singly Cabibbo-suppressed hadronic decays of Λ_c^+* , *Phys. Rev. D* **97** (2018) 074028.
- [11] J. Zou, F. Xu, G. Meng, and H. Y. Cheng, *Two-body hadronic weak decays of antitriplet charmed baryons*, *Phys. Rev. D* **101** (2020) 014011.
- [12] W. Wang, F. S. Yu, and Z. X. Zhao, *Weak decays of doubly heavy baryons: the $1/2 \rightarrow 1/2$ case*, *Eur. Phys. J. C* **77** (2017) 781.
- [13] C. Q. Geng, Y. K. Hsiao, C. W. Liu, and T. H. Tsai, *Antitriplet charmed baryon decays with $SU(3)$ flavor symmetry*, *Phys. Rev. D* **97** (2018) 073006.
- [14] S. Kurokawa and E. Kikutani, *Overview of the KEKB accelerators*, *Nucl. Instrum. Meth. A* **499** (2003) 1.
- [15] T. Abe *et al.*, *Achievements of KEKB*, *PTEP* **2013** (2013) 03A001.
- [16] BELLE collaboration, *Physics achievements from the Belle experiment*, *PTEP* **2012** (2012) 04D001.
- [17] BELLE collaboration, *The Belle detector*, *Nucl. Instrum. Meth. A* **479** (2002) 117.
- [18] D. J. Lange, *The EvtGen particle decay simulation package*, *Nucl. Instrum. Meth. A* **462** (2001) 152.

- [19] R. Brun *et al.*, *GEANT 3.21*, CERN-DD-EE/84-1 (1987).
- [20] T. Sjöstrand, S. Mrenna, and P. Skands, *A brief introduction to PYTHIA 8.1*, *Comput. Phys. Commun.* **178** (2008) 852.
- [21] PARTICLE DATA GROUP collaboration, *Review of particle physics (2021)*, *PTEP* **2020** (2020) 083C01.
- [22] E. Barberio and Z. Was, *PHOTOS: A universal Monte Carlo for QED radiative corrections. Version 2.0*, *Comput. Phys. Commun.* **79** (1994) 291.
- [23] X. Y. Zhou, S. X. Du, G. Li, and C. P. Shen, *TopoAna: A generic tool for the event type analysis of inclusive Monte-Carlo samples in high energy physics experiments*, *Comput. Phys. Commun.* **258** (2021) 107540.
- [24] G. Punzi, *Sensitivity of searches for new signals and its optimization*, arXiv:physics/0308063.
- [25] E. Nakano, *Belle PID*, *Nucl. Instrum. Meth. A* **494** (2002) 402.
- [26] K. Hanagaki, H. Kakuno, H. Ikeda, T. Iijima, and T. Tsukamoto, *Electron identification in Belle*, *Nucl. Instrum. Meth. A* **485** (2002) 490.
- [27] M. Oreglia, *A Study of the reactions $\psi' \rightarrow \gamma\gamma\psi$* , *PhD thesis*, SLAC-R-236 (1980).
- [28] S. S. Wilks, *The Large-Sample Distribution of the Likelihood Ratio for Testing Composite Hypotheses*, *Annals Math. Statist.* **9** (1938) 60.
- [29] BESIII collaboration, *Measurement of the Matrix Element for the Decay $\eta' \rightarrow \eta\pi^+\pi^-$* , *Phys. Rev. D* **83**, 012003 (2011).
- [30] R. H. Dalitz, *CXII. On the analysis of τ -meson data and the nature of the τ -meson*, *Phil. Mag.* **44** (1953) 1068.